Pedestal Bifurcation and Resonant Field Penetration at the Threshold of Edge-Localized Mode Suppression in the DIII-D Tokamak

R. Nazikian, C. Paz-Soldan, J. D. Callen, J. S. deGrassie, D. Eldon, T. E. Evans, N. M. Ferraro, B. A. Grierson, R. J. Groebner, S. R. Haskey, C. C. Hegna, J. D. King, N. C. Logan, G. R. McKee, R. A. Moyer, M. Okabayashi, D. M. Orlov, T. H. Osborne, J-K. Park, T. L. Rhodes, M. W. Shafer, P. B. Snyder, W. M. Solomon, E. J. Strait, and M. R. Wade

Pedestal Bifurcation and Resonant Field Penetration at the Threshold of Edge-Localized Mode Suppression in the DIII-D Tokamak

R. Nazikian[1], C. Paz-Soldan[2], J.D. Callen[5], J.S. deGrassie[2], D. Eldon[3], T.E. Evans[2], N.M. Ferraro[2], B.A. Grierson[1], R.J. Groebner[2], S.R. Haskey[4], C.C. Hegna[5], J.D. King[2], N.C. Logan[1], G.R. McKee[5], R.A. Moyer[3], M. Okabayashi[1], D.M. Orlov[3], T.H. Osborne[2], J-K. Park[1], T.L. Rhodes[6], M.W. Shafer[7], P.B. Snyder[2], W.M. Solomon[1], E.J. Strait[2], M.R. Wade[2]

[1]*Princeton Plasma Physics Laboratory, PO Box 451, Princeton, NJ 08543-0451, USA*
[2]*General Atomics, PO Box 85608, San Diego, CA 92186-5608, USA*
[3]*University of California San Diego, 9500 Gilman Dr., La Jolla, CA 92093-0417, USA*
[4]*Australian National University, Canberra, ACT, Australia*
[5]*University of Wisconsin-Madison, 1500 Engineering Dr., Madison, WI 53706, USA*
[6]*University of California Los Angeles, Los Angeles, CA 90095, USA*
[7]*Oak Ridge National Laboratory, PO Box 2008, Oak Ridge, TN 37831, USA*

Rapid bifurcations in the plasma response to slowly varying n=2 magnetic fields are observed as the plasma transitions into and out of edge localized mode (ELM) suppression. The rapid transition to ELM suppression is characterized by an increase in the toroidal rotation and a reduction in the electron pressure gradient at the top of the pedestal which reduces the perpendicular electron flow to near zero. These events occur simultaneously with an increase in the inner wall magnetic response. These observations are consistent strong resonant field penetration of n=2 fields at the onset of ELM suppression, based on extended MHD simulations using measured plasma profiles. Spontaneous transitions into (and out of) ELM suppression with a static applied n=2 field indicate competing mechanisms of screening and penetration of resonant fields near threshold conditions. Magnetic measurements reveal evidence for the unlocking and rotation of tearing-like structures as the plasma transitions out of ELM suppression.

Transient events such as edge localized modes (ELMs) in fusion reactors can rapidly release up to 20% of the plasma stored-energy to the walls, leading to excessive material erosion [1]. One method to suppress ELMs is the use of resonant magnetic perturbations (RMPs) [2]. In recent years there has been rapid expansion in the use of RMPs for mitigating [3-5] and suppressing ELMs [6,7] however leading theoretical models for ELM suppression [8-10] have yet to be validated experimentally. In this Letter we explore the dynamics of ELM suppression by slowly varying the applied n=2 resonant field strength [11-13] using the in-vessel I-coils on DIII-D. Rapid bifurcations are observed in the edge profiles and magnetic response of the plasma to the slow variation in the applied field near the threshold for ELM suppression. The measurements also reveal evidence for the unlocking of edge magnetic structures in the back-transition to ELMing conditions.

These observations of pedestal bifurcations into and out of ELM suppression are phenomenological analogous to the bifurcations driven by resonant components of the intrinsic error field in the core of tokamak plasmas [14]. Such bifurcations are predicted theoretically when the error field induced torque exceeds the viscous torque due to plasma flow, leading to magnetic reconnection on low-order rational surfaces [15]. These changes are concomitant with a large reduction of the perpendicular electron flow at the rational surface [16] and an amplification of the externally measured magnetic response of the plasma. The applicability of this generic resonant field penetration paradigm for ELM suppression in DIII-D will be explored in the remainder of this Letter. The observations presented here are made possible by improved edge Thomson scattering measurements and new magnetic measurements on the inner wall of the DIII-D tokamak [17,18]. The relevant parameters for these plasmas are: Toroidal field B_T=-1.9 T, plasma current I_p=1.36 MA, major radius R=1.75 m, midplane minor radius a=0.59 m, neutral beam power P_{NBI}= 6 MW, electron cyclotron heating P_{EC}=1.0 MW, pedestal electron collisionality ν_{*e}<0.3, edge magnetic safety factor q_{95}=4.1.
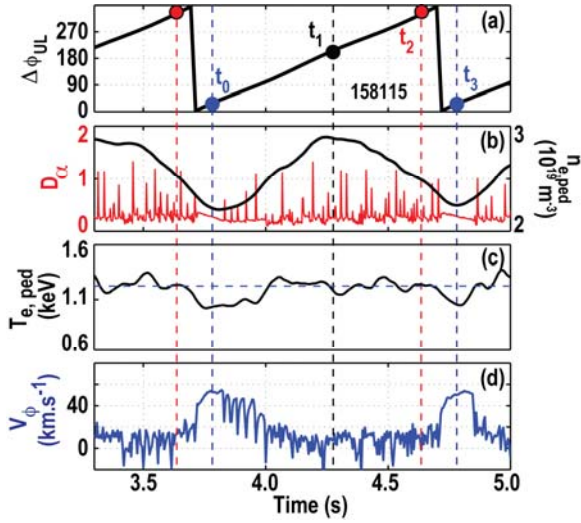
Fig. 1. Pedestal bifurcations with slowly varying resonant fields. (a) Upper/lower row I-coil relative phase (b) D_α light near the outer strike point (red) and pedestal density $n_{e,ped}$ (black), (c) pedestal electron temperature $T_{e,ped}$ (d) edge impurity velocity in the co-I_P direction.

Fig. 2. (a) Contours of T_e vs ψ_n and D_α signal (black), contours of B_{pol} (Gauss) vs time and toroidal angle for (b) n=1 inner wall (c), n=1 outer wall (d) n=2 inner wall (e) n=2 outer wall.

In these experiments on DIII-D the resonant field strength is varied slowly in order to identify the nonlinear dynamics specific to the onset of ELM suppression. In typical ELM suppression experiments in low collisionality plasmas the RMP field is rapidly applied so that density "pumpout" (density reduction due to the RMP) and ELM suppression occur on similar time scales [7]. By slowly varying the resonant field strength, the time scale for density pumpout is considerably lengthened and the detailed bifurcation dynamics of ELM suppression is revealed. The resonant field strength is slowly varied by controlling the relative phase $\Delta\phi_{UL}$ of the n=2 field between the two rows of I-coils in DIII-D [Fig. 1 of Ref. 12]. The n=2 field in the upper row of coils is rotated toroidally at 1 Hz while the n=2 field in the lower row is held fixed. The 1 s rotation period of the field in the upper row is long compared to the typical time scale for density pumpout (~100 ms) observed during the rapid application of resonant fields. The relative phase between the two rows of I-coils is shown in Fig. 1(a). For $q_{95}\approx4$ at the top of the pedestal, the peak in the edge resonant field occurs near $\Delta\phi_{UL}\approx0$ deg., with poloidal mode number $m\approx nq_{95}$ where n=2. The minimum in the resonant field occurs near $\Delta\phi_{UL}\approx180$ deg. [Fig. 13 of Ref. 12].

Near $\Delta\phi_{UL}\approx0$ the plasma transitions to the ELM suppressed state and rapid bifurcations are observed in the plasma edge profiles and magnetic response during these transitions. Narrow intervals of ELM suppression near $\Delta\phi_{UL}\approx0$ (near t_0, t_3 in Fig. 1) are observed on the deuterium-alpha (D_α) line emission from the divertor [Fig.1(b)]. The pedestal density $n_{e,ped}$ and electron
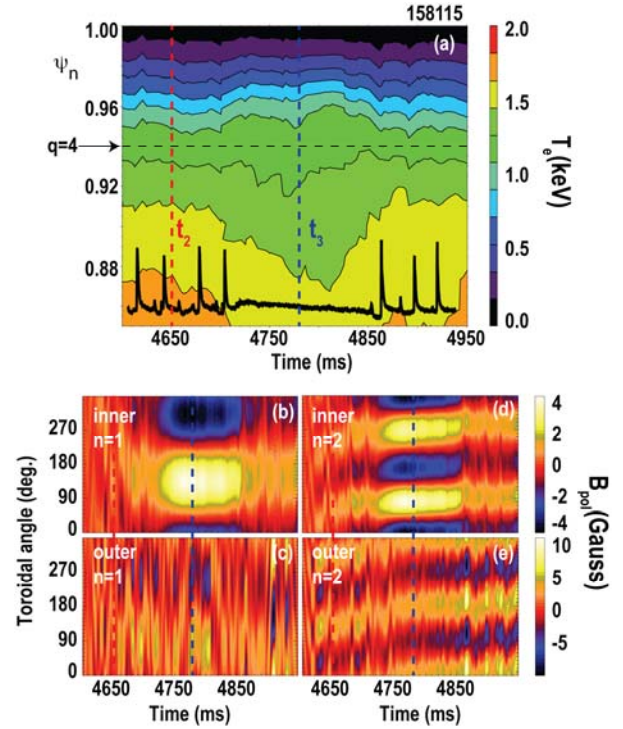
temperature $T_{e,ped}$ are obtained using hyperbolic tangent fits of edge Thomson scattering profiles [19]. Rapid drops of ~20% in $T_{e,ped}$ are seen at the transition to ELM suppression [Fig. 1(c)] whereas $n_{e,ped}$ evolves gradually with the strength of the applied resonant field as shown in Fig. 1(b). A rapid increase in the carbon toroidal velocity V_ϕ near normalized poloidal flux $\psi_n\approx0.97$ is also seen at the transition to ELM suppression in Fig. 1(d). As the phase $\Delta\phi_{UL}$ continues to increase away from $\Delta\phi_{UL}\approx0$, the strength of the resonant field decreases and the plasma experiences a pedestal bifurcation out of ELM suppression, returning to ELMing conditions.

The plasma in the short intervals of ELM suppression in Fig. 1 exhibits rapid flattening of the temperature at the top of the pedestal together with a strong nonlinear increase in the magnetic response near the midplane on the inner wall. [See Ref. 18 for the geometry of the inner and outer wall magnetic sensors.] Figure 2(a) shows a contour plot of the edge electron temperature T_e averaged over ≈20 ms and Figs. 2(b-e) show contours of the poloidal field strength B_{pol} measured near the midplane on the inner wall of DIII-D. The data of Fig. 2 corresponds to a narrow 350 ms interval around ELM suppression time t_3 in Fig. 1. The T_e contours from Thomson scattering are overlaid with the divertor D_α signal. The reduction in the gradient of T_e at the top of the pedestal can be seen by the spreading of the temperature contours around the q=4
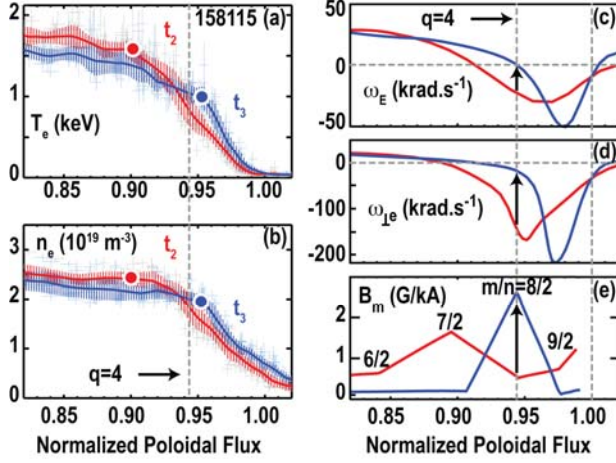
Fig. 3. (a) T_e, (b) n_e vs ψ_n averaged over 50 ms before ELM suppression (red) and during ELM suppression (blue), (c) the ExB frequency, (d) the perpendicular electron frequency (e) the n=2 resonant magnetic field strength on edge rational surfaces as calculated by M3D-C1. The circles in (a,b) denote the location at the top of the pedestal.

Fig. 4. Spontaneous bifurcations into and out of ELM suppression with static n=2 fields. (a) D_α at the outer strike point, (b) density fluctuation power spectra measured using BES at $\psi_n \approx 0.94$, (c) impurity toroidal rotation at the plasma edge, (d) n=2 B_{pol} on inner wall. Blue vertical lines indicate periods of ELM suppression, red indicates ELMing phase.

rational surface. The T_e profile change occurs with minimal change in $n_{e,ped}$ in the same interval [Fig. 1(b)], consistent with a large increase in the electron thermal transport at the top of the pedestal. Interestingly, the plasma magnetic response during ELM suppression shows increased n=1 and n=2 fields near the midplane on the inner wall [Figs. 2(b,d)] but no large increase near the midplane on the outer wall [Figs. 2(c,e)]. The presence of an n=1 magnetic component accompanying the n=2 response on the inner wall is surprising since no significant n=1 field is being applied with the I-coils. The n=1 response may be due to the penetration of resonant components of the intrinsic error field or it may be due to a coalescence instability following the penetration of the n=2 resonant field [20].

Strong n=2 resonant field penetration is predicted for the profiles measured in the ELM suppressed phase as shown in Fig. 3. Figures 3(a,b) shows T_e and n_e profiles taken immediately before (red) and during ELM suppression (blue) corresponding to the times t_2, t_3 in Fig. 1, respectively. A gradient reduction is observed in T_e and n_e at the q=4 rational surface at the top of the pedestal along with a reduction of the pedestal width. The electron pedestal density $n_{e,ped}$ in Fig. 3(b) decreases by ~10% while $T_{e,ped}$ drops by about ~30% at the transition to ELM suppression. The increase in edge carbon rotation V_ϕ in the direction of the plasma current and the reduction in the pressure gradient at the top of the pedestal leads to a large increase in the radial electric field E_r from a large negative value to near zero at the q=4 rational surface. Figure 3(c) shows the change in the ExB frequency $\omega_E = -E_r/RB_\theta$ measured using carbon line radiation, showing a narrower
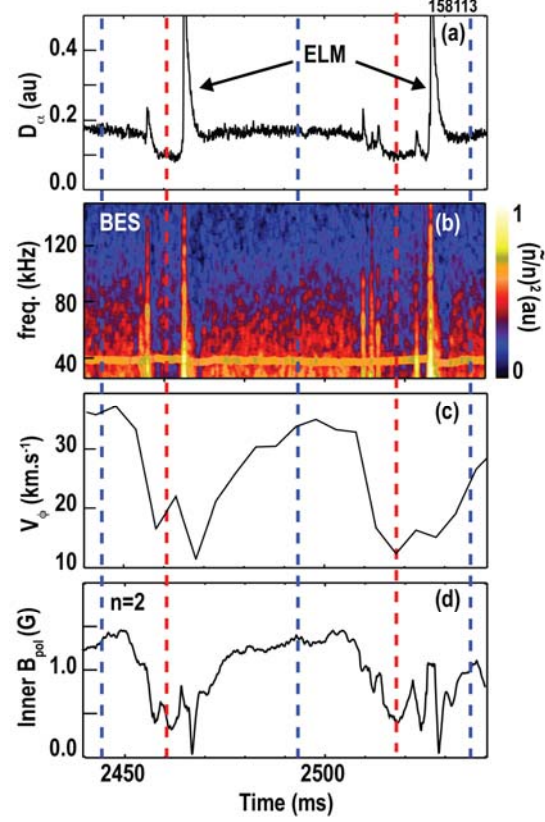
and deeper well in E_r in the ELM suppressed phase. These changes lead to a large increase in the perpendicular electron frequency $\omega_{\perp e}$ from a large negative value to near zero as indicated in Fig. 3(d) where $\omega_{\perp e} = \omega_E + \omega_{*e}$ and $\omega_{*e} = -(n_e e RB_\theta)^{-1} \times (dp_e/dr)$ is the electron diamagnetic frequency. The rapid reduction in the temperature gradient and reduction in the magnitude of ω_E and $\omega_{\perp e}$ at the q=4 rational surface at the onset of ELM suppression are consistent with the phenomenology and theory of resonant field penetration. Linear, single-fluid simulations using the M3D-C1 code [9] shows strong enhancement of the m=8/n=2 resonant field component at the q=4 rational surface in the ELM suppressed phase [Fig 3(e)], during which $\omega_{\perp e}$ and ω_E are close to zero near this rational surface. The calculated resonant field at this surface is much smaller in the ELMing phase, when $\omega_{\perp e}$ and ω_E have large negative values at the rational surface. In these single-fluid calculations the rotation is taken to be the measured ω_E profile. The linear calculation yields a resonant field strength ≈ 8 Gauss, or $\delta B/B \sim 4 \times 10^{-4}$ corresponding to an estimated island width of ~2 cm. However the linear
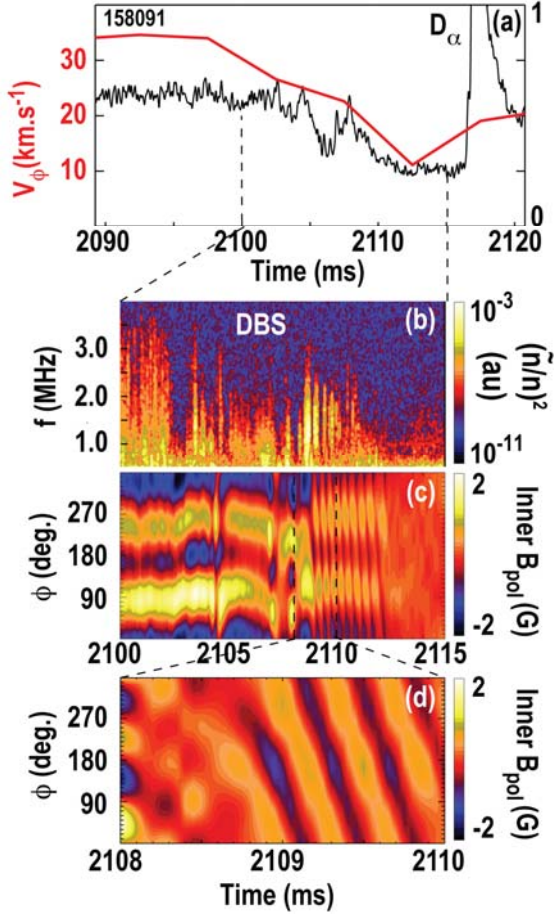
Fig. 5 During the back transition to ELMing conditions: (a) edge impurity rotation (red) and D_α at outer strike point, (b) spectrogram of DBS signal (c) contours of B_{pol} (G) vs time and toroidal angle on inner wall, (d) contours of the AC coupled B_{pol} (G) on the inner wall.

calculation of the island width is likely a significant overestimate of the actual width of the reconnection region based on extensive measurements of temperature profiles at the top of the pedestal [see the finite temperature gradient in the pedestal from Fig. 3(a) and the temperature profiles for n=3 fields in Ref. 21]. Nonlinear simulations will be needed in the future to address the width of the reconnection region in ELM suppressed plasmas. We note that strong hysteresis is not evident in the resonant field strength required for the transition into and out of ELM suppression (Fig. 1), whereas hysteresis is a prediction of the theory for a fixed toroidal viscosity [15].

In related experiments, stationary n=2 resonant fields near the threshold of ELM suppression with $\Delta\phi_{UL}\approx0$ produce spontaneous transitions into and out of ELM suppression. The pedestal profile during these spontaneous bifurcations, observed with static n=2 fields on the I-coils, are similar to the profiles seen with slowly varying fields

in Figs. 1-3. Figure 4 shows two bifurcation cycles observed with static fields, [ELM suppression (blue dashed line) → back-transition to ELMing conditions (red dashed line) → ELM event → repeat]. The bifurcations in the carbon toroidal rotation [Fig. 4(c)] and the inner-wall magnetic response [Fig. 4(d) are evident and very similar to the bifurcations seen in Figs. 1-2. In addition the temperature and density profiles for the data of Fig. 4 are essentially identical to the profiles before and during ELM suppression in Figs. 3(a,b). Edge broadband density fluctuations [Fig. 4(b)] with $k_\perp\rho_i\approx0.5$ measured using beam emission spectroscopy (BES) [22] indicate elevated density fluctuation levels of ≈1.4% in the ELM suppressed phase relative to ≈0.7% in the back-transition to ELMing conditions with no change in the applied field strength. From Fig. 4(b), transient bursts of density fluctuations are observed at the back-transition to ELMing conditions. Note that a 40 kHz MHD oscillation appears in the edge BES data however the oscillation is due to a core MHD mode and is unaffected by changes in the pedestal. The enhanced fluctuation level during ELM suppression coincides with reduced temperature and density gradients at the q=4 rational surface [Figs. 3(a,b)] and increased D_α signal [Fig. 4(a)] indicating enhanced recycling at the divertor. The increase in the broadband density fluctuation level in the ELM suppressed phase is consistent with theoretical predictions of resonant field effects on turbulence [23].

Analysis of the inner wall magnetic signals reveals the unlocking, rotation and damping of edge tearing-like structures when the plasma transitions out of ELM suppression, analogous to the transition from resonant field penetration to resonant field screening [14,15]. Figure 5 shows a back-transition out of ELM suppression with a quiescent period of about 7 ms before the first ELM. Figure 5(a) reveals a precipitous drop in the edge carbon rotation V_ϕ and D_α emission preceding the ELM. The reduction in the D_α emission after 2108 ms indicates reduced recycling at the outer strike point, characteristic of the back transition to ELMing conditions. Figure 5(b) is a qualitative indicator of high-k (kρ$_i$~1.3) density fluctuations near the top of the H-mode pedestal measured using the Doppler backscattering (DBS) system [24]. The decrease in the broadband fluctuations correlates with the reduction in the D_α emission prior to the ELM onset. Interestingly, transient bursts of broadband fluctuations near 2108 ms in Fig. 5(b) coincide with the unlocking of tearing-like structures shown in the contour plot of B_{pol}. Both the n=1 and n=2 inner wall fields decay prior to the ELM onset [Fig. 5(c)], coincident with the reduction in broadband fluctuations and D_α emission. Figure 5(d) shows a 2 ms interval of B_{pol} contours filtered to remove slowly varying features, revealing that the n=1 mode is the dominant rotating component of the magnetic signal on the

4

inner wall starting at 2109 ms. The n=2 component can exhibit toroidal phase jumps as it decays but does not readily rotate, possibly due to the effective entrainment of the mode to the applied n=2 field. The unlocked mode oscillates at ≈3 kHz for several cycles before disappearing. The low mode frequency and correlation to edge D_α events and edge fluctuation bursts reveals the edge localization of the magnetic features. Core MHD activity typically occurs above 20 kHz in these rapidly rotating plasmas [Fig. 4(b)], unlike the modes observed here. The unlocking and decay of the magnetic signals is consistent with the screening of tearing-like structures as the magnitude of $\omega_{\perp e}$ increases at the back-transition to ELMing conditions. These spontaneous bifurcations into and out of ELM suppression with static I-coil fields indicate competing mechanisms of resonant field penetration and screening near threshold conditions. We speculate here that the fluctuation bursts preceding the ELMs may facilitate the screening of resonant fields and precipitate the back-transition to ELMing conditions.

In summary, recent experiments combined with improved profile and magnetic measurements indicate that resonant field penetration triggers the onset of ELM suppression in the DIII-D tokamak. Inner wall magnetic sensors reveal evidence for the unlocking, rotation and screening of tearing-like structures at the back-transition to ELMing conditions. Ultimately, ELM suppression will need to be understood in terms of the combined effects resonant and non-resonant fields have on edge stability [25] and transport [26]. Future theoretical work is required to understand the threshold condition and bifurcation dynamics of ELM suppression in order to predict ELM suppression requirements in future experiments.

[1]   A. Loarte *et al*., Nucl. Fusion **54**, 033007 (2014).
[2]   T. E. Evans *et al.*, Nature Physics **2**, 419 (2006).
[3]   A. Kirk *et al.*, Nucl. Fusion **50**, 034008 (2010).
[4]   Y. Liang *et al.*, Nucl. Fusion **53**, 073036 (2013).
[5]   W. Suttrop *et al.*, Phys. Rev. Lett. **106**, 225004 (2011).
[6]   Y. Jeon *et al.*, Phys. Rev. Lett. **109**, 035004 (2012).
[7]   T.E. Evans *et al.*, Nucl. Fusion **53**, 093029 (2013).
[8]   M.R. Wade *et al.*, Nucl. Fusion **55**, 023002 (2015).
[9]   N.M. Ferraro, Phys. Plasmas **19**, 056105 (2012).
[10]   P.B. Snyder *et al.*, Phys. Plasmas **19**, 056115 (2012).
[11]   M.J. Lanctot *et al.*, Nucl. Fusion **53**, 083019 (2013).
[12]   S.R. Haskey *et al.*, Plasma Phys. Control. Fusion **56**, 035005 2014.
[13]   C. Paz-Soldan *et al.*, "Observation of multi-component plasma response and its relationship to density pump out and edge localized mode suppression," submitted to Phys. Rev. Lett. (2014).
[14]   T.C. Hender *et al.*, Nucl. Fusion **32**, 2091 (1992).
[15]   R. Fitzpatrick, Nucl. Fusion **33**, 1049 (1993).
[16]   F.L. Waelbroeck, Phys. Plasmas **10**, 4040 (2003).
[17]   D. Eldon *et al.*, Rev. Sci. Instrum. **83**, 10E343 (2012).
[18]   J.D. King *et al.*, Rev. Sci. Instrum. **85**, 083503 (2014).
[19]   R.J. Groebner, *et al.,* Nucl. Fusion **41**, 1789 (2001).
[20]   A. Bondeson, Phys. Rev. Lett. **51**, 1668 (1983).
[21]   R. Nazikian, *et al.*, in Proceedings of 25th IAEA Fusion Energy Conf. (Saint Petersburg, Russia, 2014) paper EX/1-1.
[22]   G.R. McKee *et al.*, Nucl. Fusion **53**, 113011 (2013).
[23]   M. Leconte and P.H. Diamond, Phys. Plasmas **18**, 082309 (2011).
[24]   W.A. Peebles *et al.*, Rev. Sci. Instrum. **81**, 10D902 (2010).
[25]   T.M. Bird and C.C. Hegna, Phys. Plasmas **21**, 100702 (2014).
[26]   J.D. Callen *et al.,* Nucl. Fusion **53**, 113015 (2013).